Wideband Active RISs: Architecture, Modeling, and Beamforming Design

Jida Zhang, Zhiyi Li, and Zijian Zhang

***Abstract*—Reconfigurable intelligent surfaces (RISs) have become a candidate for future 6G networks. The concept of active RISs has been recently proposed to overcome the multiplicative fading of RIS aided reflected links. However, due to the frequency-selective channels, the narrowband active RISs suffer from a large performance loss in wideband scenarios. To address this issue, in this letter, we propose wideband active RISs, including their architecture, modeling, and beamforming design. Specifically, the key idea of wideband active RISs is to divide all subcarriers into several groups and the subcarriers in each group are configured by a single amplifying and phase-shift circuit. Based on this architecture, we derive the frequency-domain channel model and noise model of a wideband active RIS aided communication system. Then, we formulate a beamforming design problem for sum-rate maximization, and a joint transmit precoding and reflect beamforming algorithm is proposed to solve the problem. Simulation results verify the significant performance improvement of the proposed wideband RISs in wideband scenarios.**

I. Introduction

In recent years, the emerging reconfigurable intelligent surface (RIS) technology has attracted extensive interest in the wireless communication community [1]. By properly configuring the phase shifts of passive RIS elements, the signals from transmitters can be passively reflected toward flexible directions [2]. Thanks to their high array gain and low cost, RISs are expected to improve the capacity and increase the energy efficiency (EE) of wireless networks [3]. Despite these advantages, due to the "multiplicative fading" effect, passive RISs can hardly achieve visible gains in scenarios with strong direct links, and lots of RIS elements are required to compensate for this loss. To address this issue, the concept of active RISs has been recently proposed [4]. Different from passive RISs that only reflect signals passively, the active RISs can actively amplify the reflected signals by integrating reflection-type power amplifiers [5]. Currently, active RISs have been studied in many applications such as cell-free networks [6] and secure transmissions [7].

Although active RISs have been studied in many applications, most existing works only focus on narrowband scenarios, where only one narrowband beamformer is designed for the single carrier [4]. In wideband scenarios, the amplitude and phase shift of reflected signals will vary with the frequencies of incident signals [8], and a new element design is proposed to achieve broader bandwidth to avoid this effect [9]. However, since the narrowband beamformer still cannot well match all subcarriers simultaneously due to the frequency-selectivity of wideband channel [10], the spectrum efficiency (SE) is reduced [11]. To increase the SE, an idea is to enable RISs to adjust the reflection coefficients on multiple subcarriers independently, i.e., the wideband beamforming. To achieve this goal, the author in [12] has proposed to integrate multiple phase-shift circuits working at different frequencies in each element. In this way, passive RIS is able to use multiple independent beamformers to independently reconfigure the phase shifts on multiple subcarriers [12]. However, since the power amplifiers of active RISs cannot be adjusted independently for different frequencies, this method cannot be applied to active RISs. How to compensate for the performance loss of active RISs in wideband scenarios is still an open problem.

To solve this problem, in this letter, we propose wideband active RISs, including their architecture, modeling, and beamforming design. Specifically, the key idea of wideband active RISs is to divide all subcarriers into several groups, and the subcarriers in each group are configured by a single amplifying and phase-shift circuit. To achieve this goal, wideband active RISs integrate multiple amplifying and phase-shift circuits operating at different frequencies in each of their elements. Then, we derive the frequency-domain channel model and noise model of a wideband active RIS aided communication system. Based on these models, we formulate the beamforming design problem for sum-rate maximization, and a joint transmit precoding and reflect beamforming algorithm is proposed to solve the problem. Simulation results verify the significant performance improvement of the proposed wideband active RISs in wideband scenarios.

Notations: $\mathbb{C}$, $\mathbb{R}$, and $\mathbb{R}_+$ are the sets of complex, real and positive real numbers, respectively; $[K]$ represents the set of integers $\{1, 2, \ldots, K\}$; $\boldsymbol{A}^{\mathrm{T}}$, $\boldsymbol{A}^*$, $\boldsymbol{A}^{\mathrm{H}}$, $\boldsymbol{A}^{-1}$ denote the transpose, conjugate, conjugate-transpose and inverse of $\boldsymbol{A}$; $\boldsymbol{A}[i,j]$ denotes the (i,j)-th element of $\boldsymbol{A}$; $\mathrm{diag}(\cdot)$ denotes the block diagonal operation; $\|\cdot\|_{\mathrm{F}}$ denotes the Frobenius norm; $\Re\{\cdot\}$ denotes the real part of its argument; $\otimes$ is the Kronecker product; $\mathcal{CN}(\boldsymbol{\mu}, \boldsymbol{\Sigma})$ denotes the complex Gaussian distribution with mean $\boldsymbol{\mu}$ and variance $\boldsymbol{\Sigma}$; $\boldsymbol{I}_N$ is an $N \times N$ identity matrix.

II. Architecture Design and System Model

In this section, we introduce the architecture of the proposed wideband active RISs in Subsection II-A, and present the system model of a wideband active RIS aided communication system in Subsection II-B.

Manuscript received February 4, 2023; revised March 21, 2023; accepted April 25, 2023. Date of publication XXX XX, XXXX. This work was supported in part by the National Key Research and Development Program of China (Grant No. 2020YFB1807201), in part by the National Natural Science Foundation of China (Grant No. 62031019), and in part by the European Commission through the H2020-MSCA-ITN META WIRELESS Research Project under Grant 956256. (*Corresponding author: Zijian Zhang.*)

All authors are with the Department of Electronic Engineering, Tsinghua University, Beijing 100084, China, and also with the Beijing National Research Center for Information Science and Technology (BNRist), Beijing 100084, China (e-mail: {zhang-jd20, lizhiyi20, zhangzj20}@mails.tsinghua.edu.cn).

Digital Object Identifier 10.1109/LCOMM.2023.XXXXXXX

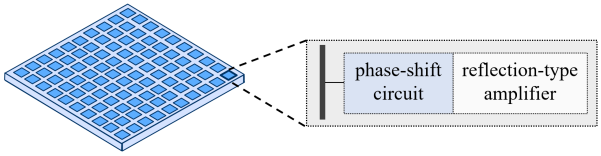

(a) Narrowband active RIS

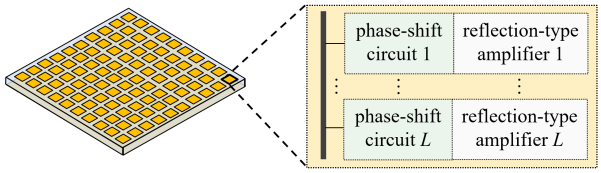

(b) Wideband active RIS

Fig. 1. Comparison between (a) narrowband active RIS and (b) wideband active RIS.

A. Architecture Design

As shown in Fig. 1 (a), the narrowband active RIS only integrates an amplifying and phase-shift circuit in each element, which means that a single beamformer is applied to all K subcarriers. This will lead to a large performance loss in orthogonal frequency division multiplexing (OFDM) system with frequency-selective channels [11].

To address this issue, we propose the architecture of wideband active RISs, as shown in Fig. 1 (b). By integrating multiple amplifying and phase-shift circuits operating at different frequencies in each element, the key idea of wideband active RISs is to divide all subcarriers into L groups ($L \leq K$) by ranking them according to their center-frequency and evenly dividing them into groups, wherein subcarriers with similar center-frequency are in the same group and can be configured by a single amplifying and phase-shift circuit. Since the subcarriers in real-world OFDM systems are scheduled and transmitted in independent time-frequency blocks, the working bandwidth of each circuit is very different. Thus, the proposed architecture is assumed to be able to avoid cross-interference between different beamformers. Multiple circuits can work together independently, each configuring the amplitude and phase shift of subcarriers in one group, and the response for other groups is neglected.

Note that, since the number of subcarriers is usually large in practice (dozens to hundreds), to obtain a compromise between performance and hardware cost, the number of groups L is usually much smaller than that of subcarriers K. In this way, each active element only needs to integrate a few amplifying and phase-shift circuits so as to reduce costs while ensuring performance. Particularly, $L = K$ means that the signal of each subcarrier can be reconfigured independently, i.e., the maximum control degrees of freedom (DoFs). $L = 1$ means that all subcarriers share the same beamformer, thus the wideband architecture degenerates to the conventional architecture of narrowband active RISs.

B. System Model

We consider a wideband active RIS aided multiuser multi-input single-output OFDM (MU-MISO-OFDM) communication system with P single-antenna users and K subcarriers with the same bandwidth. The base station (BS) is equipped with N_t antennas and the RIS comprises M elements. Indices of users, subcarriers, BS antennas and RIS elements are denoted by sets $[P]$, $[K]$, $[N_t]$ and $[M]$, respectively.

1) Transmit signal: The time-domain transmit signal $\widetilde{\boldsymbol{s}}$ is given by

$$\widetilde{\boldsymbol{s}} = \left(\boldsymbol{D}_K^{\mathrm{H}} \otimes \boldsymbol{I}_{N_t}\right) \boldsymbol{W} \boldsymbol{s}, \tag{1}$$

where $\boldsymbol{s} = [\boldsymbol{s}_1^{\mathrm{T}}, \ldots, \boldsymbol{s}_K^{\mathrm{T}}]^{\mathrm{T}} \in \mathbb{C}^{KP}$ is the overall transmit symbol and $\boldsymbol{s}_k = [s_{1,k}, \ldots, s_{P,k}]^{\mathrm{T}} \in \mathbb{C}^{P}$ is the symbol via the k-th subcarrier with $\mathbb{E}\{\boldsymbol{s}_k \boldsymbol{s}_k^{\mathrm{H}}\} = \boldsymbol{I}_P, \forall k \in [K]$. $\boldsymbol{W} = \mathrm{diag}(\boldsymbol{W}_1, \ldots, \boldsymbol{W}_K)$ where $\boldsymbol{W}_k = [\boldsymbol{w}_{1,k}, \ldots, \boldsymbol{w}_{P,k}] \in \mathbb{C}^{N_t \times P}$ is the BS precoding matrix via the k-th subcarrier; $\boldsymbol{D}_K \in \mathbb{C}^{K \times K}$ is discrete Fourier transform (DFT) matrix.

2) Channel: Assume OFDM modulation at the BS with a cyclic prefix (CP) of length L_{cp}, and the wideband channel is modeled as a L_0-tap ($L_0 \leq L_{\mathrm{cp}}$) finite impluse response (FIR). The FIR of the direct link between the BS and the p-th user is $\{\widetilde{\boldsymbol{h}}_{p,0}, \ldots, \widetilde{\boldsymbol{h}}_{p,L_1-1}\}$, where $\widetilde{\boldsymbol{h}}_{p,l} \in \mathbb{C}^{N_t}, \forall l \in \{0, \ldots, L_1 - 1\}$ is assumed to follow the exponential power-delay feature, i.e., $\widetilde{\boldsymbol{h}}_{p,l} = \sqrt{\zeta_p \frac{1-\tau}{1-\tau^{L_1}}} \tau^{l/2} \boldsymbol{\nu}_p$, where τ and ζ_p are decreasing factor and path loss, respectively. $\boldsymbol{\nu}_p \sim \mathcal{CN}(\boldsymbol{0}_{N_t}, \boldsymbol{I}_{N_t})$ is the small scale fading [13]. Similarly, the wideband channel from the BS to the RIS is $\{\widetilde{\boldsymbol{G}}_0, \ldots, \widetilde{\boldsymbol{G}}_{L_2-1}\}$, where $\widetilde{\boldsymbol{G}}_l \in \mathbb{C}^{M \times N_t}$ and that from the RIS to the p-th user is $\{\widetilde{\boldsymbol{f}}_{p,0}, \ldots, \widetilde{\boldsymbol{f}}_{p,L_3-1}\}$, where $\widetilde{\boldsymbol{f}}_{p,l} \in \mathbb{C}^{M}$. $L_0 = \max\{L_1, L_2 + L_3 - 1\}$. The time-domain channels can be efficiently estimated based on RIS aided wideband channel estimation strategies like [14].

3) RIS beamforming: We let $\boldsymbol{\Psi}_k = \mathrm{diag}(p_{k,1} e^{j\theta_{k,1}}, \ldots, p_{k,M} e^{j\theta_{k,M}})$ denote the reflection coefficient matrix of the active RIS for the k-th subcarrier, where $p_{k,m} \in \mathbb{R}_+$ and $\theta_{k,m} \in [-\pi, \pi]$ are the amplifying factor and phase-shift of the m-th element for the k-th subcarrier, respectively, $\forall k \in [K]$ and $\forall m \in [M]$. All K subcarriers are divided into L groups. Let $[L]$ denote the set of group indices and $\mathcal{K}_l$ denote the indices of subcarriers from the l-th group, i.e., $\mathcal{K}_l$ is $\{(l-1)K/L + 1, \ldots, lK/L\}$. Thus, $\boldsymbol{\Psi}^{(l)} \triangleq \boldsymbol{\Psi}_k, \forall k \in \mathcal{K}_l$ is the RIS reflection coefficient matrix for the l-th group, and the overall reflection coefficient matrix for all the subcarriers is given by $\boldsymbol{\Psi} = \mathrm{diag}(\boldsymbol{\Psi}_1, \ldots, \boldsymbol{\Psi}_K) = \mathrm{diag}(\boldsymbol{I}_{K/L} \otimes \boldsymbol{\Psi}^{(1)}, \ldots, \boldsymbol{I}_{K/L} \otimes \boldsymbol{\Psi}^{(L)}) \in \mathbb{C}^{MK \times MK}$. In time-domain, it can be expressed as $\widetilde{\boldsymbol{\Psi}} = (\boldsymbol{D}_K^{\mathrm{H}} \otimes \boldsymbol{I}_M) \boldsymbol{\Psi} (\boldsymbol{D}_K \otimes \boldsymbol{I}_M)$.

4) Received signal: In time-domain, the received signal at the p-th user is given by

$$\widetilde{\boldsymbol{y}}_p = (\widetilde{\boldsymbol{H}}_p + \widetilde{\boldsymbol{F}}_p \widetilde{\boldsymbol{\Psi}} \widetilde{\boldsymbol{G}})(\boldsymbol{D}_K^{\mathrm{H}} \otimes \boldsymbol{I}_{N_t}) \boldsymbol{W} s + \widetilde{\boldsymbol{F}}_p \widetilde{\boldsymbol{\Psi}} \widetilde{\boldsymbol{v}} + \widetilde{\boldsymbol{n}}_p, \tag{2}$$

where the channel $\widetilde{\boldsymbol{H}}_p \in \mathbb{C}^{K \times KN_t}$, $\widetilde{\boldsymbol{G}} \in \mathbb{C}^{MK \times KN_t}$ and $\widetilde{\boldsymbol{F}}_p \in \mathbb{C}^{K \times KM}$ are block circulant matrices with zero-padded FIRs $[\widetilde{\boldsymbol{h}}_{p,0}, \ldots, \widetilde{\boldsymbol{h}}_{p,L_1-1}]^{\mathrm{H}}$, $[\widetilde{\boldsymbol{G}}_0^{\mathrm{H}}, \ldots, \widetilde{\boldsymbol{G}}_{L_2-1}^{\mathrm{H}}]^{\mathrm{H}}$ and $[\widetilde{\boldsymbol{f}}_{p,0}, \ldots, \widetilde{\boldsymbol{f}}_{p,L_3-1}]^{\mathrm{H}}$ as their first column block, respectively. $\widetilde{\boldsymbol{v}}$ and $\widetilde{\boldsymbol{n}}_p$ denote time-domain dynamic noise and static noise at the p-th user, respectively. Applying DFT, the frequency-domain received signal is given by

$$\boldsymbol{y}_p = \boldsymbol{D}_K (\widetilde{\boldsymbol{H}}_p + \widetilde{\boldsymbol{F}}_p \widetilde{\boldsymbol{\Psi}} \widetilde{\boldsymbol{G}})(\boldsymbol{D}_K^{\mathrm{H}} \otimes \boldsymbol{I}_{N_t}) \boldsymbol{W} s + \boldsymbol{D}_K (\widetilde{\boldsymbol{F}}_p \widetilde{\boldsymbol{\Psi}} \widetilde{\boldsymbol{v}} + \widetilde{\boldsymbol{n}}_p). \tag{3}$$

The equivalent frequency-domain channel $\bar{\boldsymbol{H}}_p \triangleq \boldsymbol{D}_K (\widetilde{\boldsymbol{H}}_p + \widetilde{\boldsymbol{F}}_p \widetilde{\boldsymbol{\Psi}} \widetilde{\boldsymbol{G}})(\boldsymbol{D}_K^{\mathrm{H}} \otimes \boldsymbol{I}_{N_t})$ can be further simplified as block diagonal matrices as shown in [15]. Here we give a general proof.

Lemma 1. *Matrices that have a structure of* $\boldsymbol{A} = (\boldsymbol{D}_K \otimes \boldsymbol{I}_M)\widetilde{\boldsymbol{A}}(\boldsymbol{D}_K^{\mathrm{H}} \otimes \boldsymbol{I}_N)$ *is block diagonized, i.e.,* $\boldsymbol{A} = \mathrm{diag}(\boldsymbol{A}_1, \ldots, \boldsymbol{A}_K)$*, where* $\widetilde{\boldsymbol{A}} \in \mathbb{C}^{MK \times KN}$ *is a block circulant matrix whose first column block is* $[\hat{\boldsymbol{A}}_1^{\mathrm{H}}, \ldots, \hat{\boldsymbol{A}}_K^{\mathrm{H}}]^{\mathrm{H}}$ *with each block being* $\hat{\boldsymbol{A}}_k \in \mathbb{C}^{M \times N}$*.* $\boldsymbol{A}_k \in \mathbb{C}^{M \times N}$ *is defined as below and* $\boldsymbol{D}_K \in \mathbb{C}^{K \times K}$ *is the DFT matrix.*

Proof: By some algebraic calculations, we obtain

$$\begin{aligned}
\boldsymbol{A} &= (\boldsymbol{D}_K \otimes \boldsymbol{I}_M)\widetilde{\boldsymbol{A}}(\boldsymbol{D}_K^{\mathrm{H}} \otimes \boldsymbol{I}_N) \\
&\overset{(a)}{=} \boldsymbol{\Upsilon}_1 \times \left(\boldsymbol{\Upsilon}_1^{\mathrm{T}}(\boldsymbol{D}_K \otimes \boldsymbol{I}_M)\boldsymbol{\Upsilon}_1\right) \times \left(\boldsymbol{\Upsilon}_1^{\mathrm{T}}\widetilde{\boldsymbol{A}}\boldsymbol{\Upsilon}_2\right) \times \\
&\quad \left(\boldsymbol{\Upsilon}_2^{\mathrm{T}}(\boldsymbol{D}_K^{\mathrm{H}} \otimes \boldsymbol{I}_N)\boldsymbol{\Upsilon}_2\right) \times \boldsymbol{\Upsilon}_2^{\mathrm{T}} \\
&\overset{(b)}{=} \boldsymbol{\Upsilon}_1(\boldsymbol{I}_M \otimes \boldsymbol{D}_K)\begin{bmatrix} \widetilde{\boldsymbol{A}}_{1,1} & \ldots & \widetilde{\boldsymbol{A}}_{1,N} \\ \vdots & \ddots & \vdots \\ \widetilde{\boldsymbol{A}}_{M,1} & \ldots & \widetilde{\boldsymbol{A}}_{M,N} \end{bmatrix}(\boldsymbol{I}_N \otimes \boldsymbol{D}_K^{\mathrm{H}})\boldsymbol{\Upsilon}_2^{\mathrm{T}} \\
&= \boldsymbol{\Upsilon}_1 \begin{bmatrix} \boldsymbol{D}_K\widetilde{\boldsymbol{A}}_{1,1}\boldsymbol{D}_K^{\mathrm{H}} & \ldots & \boldsymbol{D}_K\widetilde{\boldsymbol{A}}_{1,N}\boldsymbol{D}_K^{\mathrm{H}} \\ \vdots & \ddots & \vdots \\ \boldsymbol{D}_K\widetilde{\boldsymbol{A}}_{M,1}\boldsymbol{D}_K^{\mathrm{H}} & \ldots & \boldsymbol{D}_K\widetilde{\boldsymbol{A}}_{M,N}\boldsymbol{D}_K^{\mathrm{H}} \end{bmatrix}\boldsymbol{\Upsilon}_2^{\mathrm{T}} \\
&\overset{(c)}{=} \boldsymbol{\Upsilon}_1 \begin{bmatrix} \boldsymbol{\Lambda}_{1,1} & \ldots & \boldsymbol{\Lambda}_{1,N} \\ \vdots & \ddots & \vdots \\ \boldsymbol{\Lambda}_{M,1} & \ldots & \boldsymbol{\Lambda}_{M,N} \end{bmatrix}\boldsymbol{\Upsilon}_2^{\mathrm{T}} \overset{(d)}{=} \mathrm{diag}(\boldsymbol{A}_1, \ldots, \boldsymbol{A}_K),
\end{aligned} \tag{4}$$

where (a) holds by inserting column permutation matrices $\boldsymbol{\Upsilon}_1\boldsymbol{\Upsilon}_1^{\mathrm{T}} = \boldsymbol{I}_{KM}$ and $\boldsymbol{\Upsilon}_2\boldsymbol{\Upsilon}_2^{\mathrm{T}} = \boldsymbol{I}_{KN}$; (b) holds by defining circulant submatrices $\widetilde{\boldsymbol{A}}_{m,n}[a,b] = \widetilde{\boldsymbol{A}}[m + (a-1)M, n + (b-1)N], \forall a, b \in [K], m \in [M]$ and $n \in [N]$; (c) holds due to the fact that circulant matrices can be diagonalized by DFT matrix, and (d) holds by defining $\boldsymbol{A}_k \in \mathbb{C}^{M \times N}$ as $\boldsymbol{A}_k[m,n] = \boldsymbol{\Lambda}_{m,n}[k,k]$, $\forall m \in [M], n \in [N]$ and $k \in [K]$. ■

After expanding the RIS reflection coefficient matrix as $\widetilde{\boldsymbol{\Psi}} = (\boldsymbol{D}_K^{\mathrm{H}} \otimes \boldsymbol{I}_M)\boldsymbol{\Psi}(\boldsymbol{D}_K \otimes \boldsymbol{I}_M)$, the equivalent frequency-domain channel can be simplified as

$$\begin{aligned}
\bar{\boldsymbol{H}}_p =& \underbrace{\boldsymbol{D}_K\widetilde{\boldsymbol{H}}_p(\boldsymbol{D}_K^{\mathrm{H}} \otimes \boldsymbol{I}_{N_t})}_{\mathrm{diag}(\boldsymbol{h}_{p,1}^{\mathrm{H}}, \ldots, \boldsymbol{h}_{p,K}^{\mathrm{H}})} + \underbrace{\boldsymbol{D}_K\widetilde{\boldsymbol{F}}_p(\boldsymbol{D}_K^{\mathrm{H}} \otimes \boldsymbol{I}_M)}_{\mathrm{diag}(\boldsymbol{f}_{p,1}^{\mathrm{H}}, \ldots, \boldsymbol{f}_{p,K}^{\mathrm{H}})} \times \boldsymbol{\Psi} \\
&\times \underbrace{(\boldsymbol{D}_K \otimes \boldsymbol{I}_M)\widetilde{\boldsymbol{G}}(\boldsymbol{D}_K^{\mathrm{H}} \otimes \boldsymbol{I}_{N_t})}_{\mathrm{diag}(\boldsymbol{G}_1, \ldots, \boldsymbol{G}_K)} \\
=& \mathrm{diag}(\boldsymbol{h}_{p,1}^{\mathrm{H}} + \boldsymbol{f}_{p,1}^{\mathrm{H}}\boldsymbol{\Psi}_1\boldsymbol{G}_1, \ldots, \boldsymbol{h}_{p,K}^{\mathrm{H}} + \boldsymbol{f}_{p,K}^{\mathrm{H}}\boldsymbol{\Psi}_K\boldsymbol{G}_K).
\end{aligned} \tag{5}$$

where the frequency-domain channels $\boldsymbol{h}_{p,k}$, $\boldsymbol{f}_{p,k}$ and $\boldsymbol{G}_k$ are defined similarly as in **Lemma 1**. The noise model can be simplified in a similar way:

$$\boldsymbol{D}_K\widetilde{\boldsymbol{F}}_p\widetilde{\boldsymbol{\Psi}}\widetilde{\boldsymbol{v}} = \mathrm{diag}(\boldsymbol{f}_{p,1}^{\mathrm{H}}\boldsymbol{\Psi}_1, \ldots, \boldsymbol{f}_{p,K}^{\mathrm{H}}\boldsymbol{\Psi}_K)\boldsymbol{v}, \tag{6}$$

where $\boldsymbol{v} = (\boldsymbol{D}_K \otimes \boldsymbol{I}_M)\widetilde{\boldsymbol{v}}$ is the frequency-domain active noise. Similarly, $\boldsymbol{n}_p = \boldsymbol{D}_K\widetilde{\boldsymbol{n}}_p$ is the frequency-domain static noise for the p-th user, and both are modeled as additive white Gaussion noise (AWGN), i.e., $\{\boldsymbol{v}, \boldsymbol{n}_p\} \sim \mathcal{CN}(\boldsymbol{0}, \{\sigma_v^2, \sigma^2\}\boldsymbol{I})$.

Applying the simplification results to (5), the received signal via the k-th subcarrier for the p-th user can be expressed concisely as

$$y_{p,k} = \bar{\boldsymbol{h}}_{p,k}^{\mathrm{H}} \sum_{j=1}^{P} \boldsymbol{w}_{j,k}s_{j,k} + \boldsymbol{f}_{p,k}^{\mathrm{H}}\boldsymbol{\Psi}_k\boldsymbol{v}_k + n_{p,k}, \tag{7}$$

wherein $\bar{\boldsymbol{h}}_{p,k}^{\mathrm{H}} \triangleq \boldsymbol{h}_{p,k}^{\mathrm{H}} + \boldsymbol{f}_{p,k}^{\mathrm{H}}\boldsymbol{\Psi}_k\boldsymbol{G}_k \in \mathbb{C}^{1 \times N_t}$ is the overall channel from the BS to the p-th user via the k-th subcarrier, $\boldsymbol{v}_k \in \mathbb{C}^K$ is the k-th block of $\boldsymbol{v}$ and $n_{p,k}$ is the k-th element of $\boldsymbol{n}_p$. Therefore, the signal-to-interference-plus-noise ratio (SINR) via the k-th subcarrier for the p-th user is given by

$$\mathrm{SINR}_{p,k} = \frac{|\bar{\boldsymbol{h}}_{p,k}^{\mathrm{H}}\boldsymbol{w}_{p,k}|^2}{\sum_{j=1, j\neq p}^{P} |\bar{\boldsymbol{h}}_{p,k}^{\mathrm{H}}\boldsymbol{w}_{j,k}|^2 + \|\boldsymbol{f}_{p,k}^{\mathrm{H}}\boldsymbol{\Psi}_k\|_{\mathrm{F}}^2\sigma_v^2 + \sigma^2}. \tag{8}$$

5) Power consumption: The BS transmit power limitation is given by $\sum_{k=1}^{K} \|\boldsymbol{W}_k\|_{\mathrm{F}}^2 \leq P_{\mathrm{BS}}^{\max}$ and the power constraint for active RIS is expressed as $P_{\mathrm{A}} = \sum_{k=1}^{K} \|\boldsymbol{\Psi}_k\boldsymbol{G}_k\boldsymbol{W}_k\|_{\mathrm{F}}^2 + \sum_{k=1}^{K} \|\boldsymbol{\Psi}_k\|_{\mathrm{F}}^2 \sigma_v^2$. It should be noted that P_{A} is the power constraint of reflected signal from active RIS and the static power consumption is not considered in this letter.

III. Beamforming Design

In this section, the sum-rate maximization problem is firstly formulated in Subsection III-A. To solve the problem, a joint transmit precoding and reflect beamforming design is proposed in Subsection III-B.

A. Problem Formulation

Under the power constraints at the BS and the active RIS as well as the grouping settings, the original sum-rate maximization problem can be formulated as follows:

$$\mathcal{P}_1 : \max_{\boldsymbol{W}, \{\boldsymbol{\Psi}_k\}} \mathcal{R} = \frac{1}{L_{\mathrm{cp}}} \sum_{k=1}^{K}\sum_{p=1}^{P} \log_2(1 + \mathrm{SINR}_{p,k}), \tag{9a}$$

$$\text{s.t.} \sum_{k=1}^{K} \|\boldsymbol{W}_k\|_{\mathrm{F}}^2 \leq P_{\mathrm{BS}}^{\max}, \tag{9b}$$

$$\sum_{k=1}^{K} \left(\|\boldsymbol{\Psi}_k\boldsymbol{G}_k\boldsymbol{W}_k\|_{\mathrm{F}}^2 + \|\boldsymbol{\Psi}_k\|_{\mathrm{F}}^2\sigma_v^2\right) \leq P_{\mathrm{A}}^{\max}, \tag{9c}$$

$$\boldsymbol{\Psi}_k = \boldsymbol{\Psi}^{(l)}, \forall k \in \mathcal{K}_l. \tag{9d}$$

The objective function of $\mathcal{P}_1$ in (9) is non-convex with highly coupled variables. An equivalent problem can be formulated based on alternating optimization (AO) and fractional programming (FP) by introducing auxiliary variables $\boldsymbol{\alpha}$ and $\boldsymbol{\beta}$:

$$\begin{aligned}
\mathcal{P}_2 : \quad & \max_{\boldsymbol{W}, \{\boldsymbol{\Psi}_k\}, \boldsymbol{\alpha}, \boldsymbol{\beta}} \hat{\mathcal{R}} = \sum_{k=1}^{K}\sum_{p=1}^{P} \left(\log\left(\frac{1 + \alpha_{p,k}}{e^{\alpha_{p,k}}}\right) + \varphi_{p,k}\right), \\
& \text{s.t. (9b), (9c), (9d),}
\end{aligned} \tag{10}$$

where $\varphi_{p,k}$ is an auxiliary function defined as

$$\begin{aligned}
\varphi_{p,k} = & 2\sqrt{1 + \alpha_{p,k}}\Re\{\beta_{p,k}^*\bar{\boldsymbol{h}}_{p,k}^{\mathrm{H}}\boldsymbol{w}_{p,k}\} - |\beta_{p,k}|^2 \times \\
& \left(\sum_{j=1}^{P} |\bar{\boldsymbol{h}}_{p,k}^{\mathrm{H}}\boldsymbol{w}_{j,k}|^2 + \|\boldsymbol{f}_{p,k}^{\mathrm{H}}\boldsymbol{\Psi}_k\|_{\mathrm{F}}^2\sigma_v^2 + \sigma^2\right).
\end{aligned} \tag{11}$$

B. Beamforming Design

As a result, $\mathcal{P}_1$'s equivalent problem $\mathcal{P}_2$ in (10) can be solved by optimizing the four variables alternatively until convergence, which is summarized in **Algorithm 1**.

Algorithm 1 Proposed joint transmit precoding and reflect beamforming algorithm

Input: $\boldsymbol{h}_{p,k}$, $\boldsymbol{f}_{p,k}$, $\boldsymbol{G}_k$, $P_{\mathrm{A}}^{\max}$, $P_{\mathrm{BS}}^{\max}$.
Output: Optimal BS precoding matrix $\boldsymbol{W}$; Optimal RIS beamforming matrix $\{\boldsymbol{\Psi}_k\}$, $\forall k \in [K]$.
1: Initialize $\boldsymbol{W}$ and $\{\boldsymbol{\Psi}_k\}$ randomly;
2: **while** no convergence of $\mathcal{R}$ **do**
3: Update $\boldsymbol{\alpha}$ by (12);
4: Update $\boldsymbol{\beta}$ by (13);
5: Update $\boldsymbol{W}$ by solving (14);
6: Update $\boldsymbol{\Psi}$ by solving (15);
7: **end while**
8: **return** $\boldsymbol{W}^\star$, $\{\boldsymbol{\Psi}_k\}^\star$, and $\mathcal{R}$.

1) Optimize $\boldsymbol{\alpha}$: After fixing the BS precoding matrix $\boldsymbol{W}$, the RIS beamforming matrix $\{\boldsymbol{\Psi}_k\}$, and the auxiliary variable $\boldsymbol{\beta}$, the optimal $\boldsymbol{\alpha}$ is derived by setting the derivative $\partial\hat{\mathcal{R}}/\partial\alpha_{p,k}$ to 0 and defining $q_{p,k} \triangleq \Re\{\beta_{p,k}^* \bar{\boldsymbol{h}}_{p,k}^{\mathrm{H}} \boldsymbol{w}_{p,k}\}$

$$\alpha_{p,k}^\star = \frac{1}{2}\left(q_{p,k}\left(1+\sqrt{4+q_{p,k}^2}\right)\right), \tag{12}$$

2) Optimize $\boldsymbol{\beta}$: After fixing the BS precoding matrix $\boldsymbol{W}$, the RIS beamforming matrix $\{\boldsymbol{\Psi}_k\}$, and the auxiliary variable $\boldsymbol{\alpha}$, the optimal $\boldsymbol{\beta}$ is derived from $\partial\hat{\mathcal{R}}/\partial\beta_{p,k} = 0$

$$\beta_{p,k}^\star = \frac{\sqrt{1+\alpha_{p,k}}}{\boldsymbol{w}_{p,k}^{\mathrm{H}}\bar{\boldsymbol{h}}_{p,k}} \cdot \frac{\mathrm{SINR}_{p,k}}{1+\mathrm{SINR}_{p,k}}. \tag{13}$$

3) Optimize $\boldsymbol{W}$: After fixing the RIS beamforming matrix $\{\boldsymbol{\Psi}_k\}$ and two auxiliary variables, the problem in (11) can be reformulated as follows

$$\mathcal{P}_3: \ \min_{\boldsymbol{w}} \ \boldsymbol{w}^{\mathrm{H}}\boldsymbol{U}\boldsymbol{w} - 2\Re\{\boldsymbol{w}^{\mathrm{H}}\boldsymbol{\nu}\}, \tag{14a}$$
$$\text{s.t. } \|\boldsymbol{w}\|_{\mathrm{F}}^2 \le P_{\mathrm{BS}}^{\max}, \tag{14b}$$
$$\boldsymbol{w}^{\mathrm{H}}\boldsymbol{V}\boldsymbol{w} \le P_{\mathrm{m}}^{\max}. \tag{14c}$$

where the following notations are introduced for simplicity:

$$P_{\mathrm{m}}^{\max} = P_{\mathrm{A}}^{\max} - \sum_{k=1}^{K}\|\boldsymbol{\Psi}_k\|_{\mathrm{F}}^2\sigma_v^2, \ \boldsymbol{\nu}_{p,k}^{\mathrm{H}} = \sqrt{1+\alpha_{p,k}}\beta_{p,k}^*\bar{\boldsymbol{h}}_{p,k}^{\mathrm{H}},$$
$$\boldsymbol{\nu} = [\boldsymbol{\nu}_{1,1}^{\mathrm{T}},\ldots,\boldsymbol{\nu}_{P,1}^{\mathrm{T}},\ldots,\boldsymbol{\nu}_{1,K}^{\mathrm{T}},\ldots,\boldsymbol{\nu}_{P,K}^{\mathrm{T}}]^{\mathrm{T}},$$
$$\boldsymbol{w} = [\boldsymbol{w}_{1,1}^{\mathrm{T}},\ldots,\boldsymbol{w}_{P,1}^{\mathrm{T}},\ldots,\boldsymbol{w}_{1,K}^{\mathrm{T}},\ldots,\boldsymbol{w}_{P,K}^{\mathrm{T}}]^{\mathrm{T}},$$
$$\boldsymbol{U}_k = \boldsymbol{I}_P \otimes \sum_{p=1}^{P}|\beta_{p,k}|^2\bar{\boldsymbol{h}}_{p,k}\bar{\boldsymbol{h}}_{p,k}^{\mathrm{H}}, \ \boldsymbol{U} = \mathrm{diag}(\boldsymbol{U}_1,\ldots,\boldsymbol{U}_K),$$
$$\boldsymbol{V}_k = \boldsymbol{I}_P \otimes \boldsymbol{G}_k^{\mathrm{H}}\boldsymbol{\Psi}_k^{\mathrm{H}}\boldsymbol{\Psi}_k\boldsymbol{G}_k, \qquad \boldsymbol{V} = \mathrm{diag}(\boldsymbol{V}_1,\ldots,\boldsymbol{V}_K).$$

$\mathcal{P}_3$ in (14) is a standard quadratically constrained quadratic program (QCQP) problem and can be solved via CVX tools.

4) Optimize $\{\boldsymbol{\Psi}_k\}$: We define $\boldsymbol{\psi}^{(l)} \triangleq [p_{k,1}e^{-j\theta_{k,1}},\ldots,p_{k,M}e^{-j\theta_{k,M}}]^{\mathrm{T}} \in \mathbb{C}^M$, $\forall k \in \mathcal{K}_l$ as the vectorized RIS beamforming matrix for the l-th group, i.e., $\boldsymbol{\Psi}^{(l)} = \mathrm{diag}((\boldsymbol{\psi}^{(l)})^{\mathrm{H}})$. After fixing $\boldsymbol{\beta}, \boldsymbol{W}$, and $\boldsymbol{\alpha}$ the problem in (11) can be reformulated as follows:

$$\mathcal{P}_4: \ \min_{\boldsymbol{\psi}} \ \boldsymbol{\psi}^{\mathrm{H}}\boldsymbol{\Xi}\boldsymbol{\psi} - 2\Re\{\boldsymbol{\psi}^{\mathrm{H}}\boldsymbol{\mu}\}, \tag{15a}$$
$$\text{s.t. } \boldsymbol{\psi}^{\mathrm{H}}\boldsymbol{\Omega}\boldsymbol{\psi} \le P_{\mathrm{A}}^{\max}. \tag{15b}$$

wherein

$$\boldsymbol{\mu}^{(l)} = \sum_{k\in\mathcal{K}_l}\sum_{p=1}^{P}\left(\sqrt{1+\alpha_{p,k}}\mathrm{diag}\left(\beta_{p,k}^*\boldsymbol{f}_{p,k}^{\mathrm{H}}\right)\boldsymbol{G}_k\boldsymbol{w}_{p,k}\right.$$
$$\left. - |\beta_{p,k}|^2\mathrm{diag}(\boldsymbol{f}_{p,k}^{\mathrm{H}})\boldsymbol{G}_k\sum_{j=1}^{P}(\boldsymbol{w}_{j,k}\boldsymbol{w}_{j,k}^{\mathrm{H}})\boldsymbol{h}_{p,k}\right),$$

$$\boldsymbol{\Xi}^{(l)} = \sum_{k\in\mathcal{K}_l}\sum_{p=1}^{P}|\beta_{p,k}|^2\left(\mathrm{diag}(\boldsymbol{f}_{p,k}^{\mathrm{H}})\mathrm{diag}(\boldsymbol{f}_{p,k})\sigma_v^2\right.$$
$$\left. + \mathrm{diag}(\boldsymbol{f}_{p,k}^{\mathrm{H}})\boldsymbol{G}_k\sum_{j=1}^{P}(\boldsymbol{w}_{j,k}\boldsymbol{w}_{j,k}^{\mathrm{H}})\boldsymbol{G}_k^{\mathrm{H}}\mathrm{diag}(\boldsymbol{f}_{p,k})\right),$$

$$\boldsymbol{\Omega}^{(l)} = \sum_{k\in\mathcal{K}_l}\sum_{p=1}^{P}\mathrm{diag}\left(\boldsymbol{G}_k\boldsymbol{w}_{p,k}\right)\left(\mathrm{diag}\left(\boldsymbol{G}_k\boldsymbol{w}_{p,k}\right)\right)^{\mathrm{H}} + \sigma_v^2\boldsymbol{I}_M,$$
$$\boldsymbol{\psi} = [(\boldsymbol{\psi}^{(1)})^{\mathrm{T}},\ldots,(\boldsymbol{\psi}^{(L)})^{\mathrm{T}}]^{\mathrm{T}}, \ \boldsymbol{\Xi} = \mathrm{diag}(\boldsymbol{\Xi}^{(1)},\ldots,\boldsymbol{\Xi}^{(L)}),$$
$$\boldsymbol{\mu} = [(\boldsymbol{\mu}^{(1)})^{\mathrm{T}},\ldots,(\boldsymbol{\mu}^{(L)})^{\mathrm{T}}]^{\mathrm{T}}, \ \boldsymbol{\Omega} = \mathrm{diag}(\boldsymbol{\Omega}^{(1)},\ldots,\boldsymbol{\Omega}^{(L)}).$$

$\mathcal{P}_4$ in (15) is also a QCQP problem which can be solved by CVX tools.

IV. Simulation Results

In this section, we present the simulation results for the proposed wideband active RISs. The simulation setup is provided in Subsection IV-A and the numerical results are given in Subsection IV-B.

A. Simulation Setup

In order to evaluate the effectiveness of the proposed joint transmit precoding and reflect beamforming design, simulation results are presented for passive RISs, narrowband active RISs and wideband active RISs with different numbers of subcarrier groups aided MU-MISO-OFDM systems, respectively. The parameters are set according to [15]. The number of subcarriers and delay taps of time-domain channel are set as $K = 64$ and $L_{\mathrm{cp}} = 16$. The number of RIS elements and antennas at BS and users are $M = 64$, $N_t = 4$ and $P = 3$, respectively. Path loss is set to 30 dB at a reference distance 1 m for all channels. The decreasing factor is set to $\tau = 0.5$ and the path loss exponent for the BS-RIS channel, the RIS-user channel, and the BS-user channel are set to 2.8, 2.5, and 3.5, respectively. The BS-RIS distance and the RIS-user distance are fixed as $d_{\mathrm{BR}} = 50$ m and $d_{\mathrm{RU}} = 5$ m, respectively. The distance between the BS and users ranges uniformly from $d_{\mathrm{BR}} - d_{\mathrm{RU}}$ to $d_{\mathrm{BR}} + d_{\mathrm{RU}}$. The active and static noise power are set as $\sigma_v^2 = -60$ dBm and $\sigma^2 = -70$ dBm, respectively.

B. Simulation Results

The convergence of the proposed algorithm is validated in Fig. 2. To keep the hardware complexity reasonable, we consider a limited number of groups, i.e., $L = 1, 2, 4$. The case where $L = K = 64$, which is too costly to realize, is considered only as an upper bound of the average sum-rate. Compared with the passive RIS beamforming algorithm [15] which converges within less than 5 iterations, the algorithm we proposed converges relatively slowly.

This article has been accepted for publication in IEEE Communications Letters. This is the author's version which has not been fully edited and content may change prior to final publication. Citation information: DOI 10.1109/LCOMM.2023.3274433

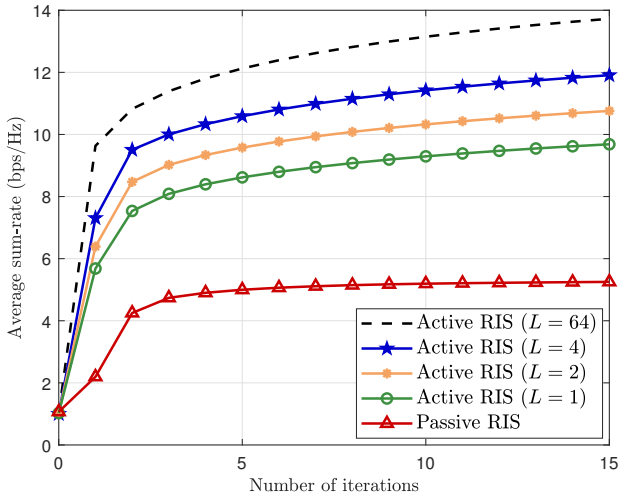

Fig. 2. Average sum-rate against number of iteration ($P_{\text{total}} = 33$ dBm)

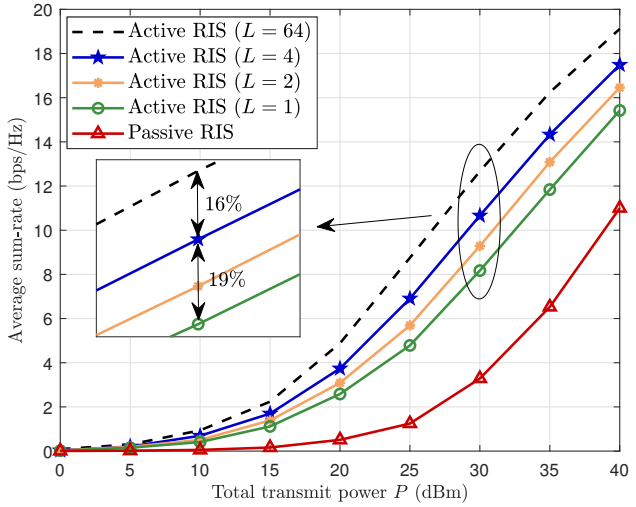

Fig. 3. Average sum-rate against total transmit power

Fig. 3 illustrates the relationship between total transmit power P_{total} and the average sum-rate. As in [4], the power constraint for passive RIS is set as $P_{\text{BS}}^{\max} = P_{\text{total}}$, and that for active RIS is set as $P_{\text{BS}}^{\max} = 0.99P_{\text{total}}$ and $P_{\text{A}}^{\max} = 0.01P_{\text{total}}$. Comparing the active RIS with $L = 64$ groups and $L = 1$ group, we can observe that the loss of narrowband active RISs can achieve more than 30%, which verifies the fact that narrowband beamformer cannot well match all subcarriers. Besides, it can also be observed that by merely dividing the subcarriers into $L = 2$ or 4 groups, about 30% and 55% of such loss can be compensated, indicating that only a few additional circuits will suffice to match the subcarriers to wideband channels.

V. Conclusions

In this letter, we have proposed wideband active RISs to compensate for the performance loss of active RISs in wideband scenarios. The proposed wideband active RISs divide all communication subcarriers into several groups and the subcarriers in each group can be configured by an independent beamformer. Then, the channel model and noise model of a wideband active RIS aided communication system is derived. Here we assume that the response of each circuit is identical to subcarriers in each group, and will leave the practical model that considers the limited bandwidth like [8] to future work. We have also developed a joint transmit precoding and reflect beamforming algorithm to maximize the sum-rate, while more metrics such as EE are left for follow-up works, where the number of groups L can also be viewed as an optimazation variable and can be designed to achieve the maximum EE.

Acknowledgment

We would like to thank Prof. Linglong Dai from Tsinghua University for his helpful discussions and constructive suggestions on wideband active RISs.

References

[1] C. Huang, A. Zappone, G. C. Alexandropoulos, M. Debbah, and C. Yuen, "Reconfigurable intelligent surfaces for energy efficiency in wireless communication," *IEEE Trans. Wireless Commun.*, vol. 18, no. 8, pp. 4157–4170, Aug. 2019.

[2] E. Basar and H. V. Poor, "Present and future of reconfigurable intelligent surface-empowered communications," *IEEE Signal Process. Mag.*, vol. 38, no. 6, pp. 146–152, Nov. 2021.

[3] Y. Zhang, C. You, and B. Zheng, "Multi-active multi-passive (MAMP)-IRS aided wireless communication: A multi-hop beam routing design," *arXiv preprint arXiv:2209.06390*, Sep. 2022.

[4] Z. Zhang, L. Dai, X. Chen, C. Liu, F. Yang, R. Schober, and H. V. Poor, "Active RIS vs. Passive RIS: Which Will Prevail in 6G?" *IEEE Trans. Commun.*, vol. 71, no. 3, pp. 1707–1725, Mar. 2023.

[5] K. Liu, Z. Zhang, L. Dai, S. Xu, and F. Yang, "Active reconfigurable intelligent surface: Fully-connected or sub-connected?" *IEEE Commun. Lett.*, vol. 26, no. 1, pp. 167–171, Jan. 2022.

[6] N. T. Nguyen, V.-D. Nguyen, H. Van Nguyen, H. Q. Ngo, S. Chatzinotas, and M. Juntti, "Spectral efficiency analysis of hybrid relay-reflecting intelligent surface-assisted cell-free massive MIMO systems," *IEEE Trans. Wireless Commun. (early access)*, Nov. 2022.

[7] Y. Li and F. Wang, "Rate maximization for active-IRS-aided secure communication networks," in *Proc. 2022 5th International Conference on Communications, Signal Processing, and their Applications (ICCSPA'22)*, Dec. 2022, pp. 1–6.

[8] H. Li, W. Cai, Y. Liu, M. Li, Q. Liu, and Q. Wu, "Intelligent reflecting surface enhanced wideband MIMO-OFDM communications: From practical model to reflection optimization," *IEEE Trans. Commun.*, vol. 69, no. 7, pp. 4807–4820, Jul. 2021.

[9] L. Wu, K. Lou, J. Ke, J. Liang, Z. Luo, J. Y. Dai, Q. Cheng, and T. J. Cui, "A Wideband Amplifying Reconfigurable Intelligent Surface," *IEEE Trans. Antennas Propagat.*, vol. 70, no. 11, pp. 10 623–10 631, Nov. 2022.

[10] G. C. Alexandropoulos, G. Lerosey, M. Debbah, and M. Fink, "Reconfigurable intelligent surfaces and metamaterials: The potential of wave propagation control for 6g wireless communications," *arXiv preprint arXiv:2006.11136*, 2020.

[11] Z. Zhang and L. Dai, "A joint precoding framework for wideband reconfigurable intelligent surface-aided cell-free network," *IEEE Trans. Signal Process.*, vol. 69, pp. 4085–4101, Aug. 2021.

[12] C. M. Moore, "Reconfigurable frequency selective surfaces," Ph.D. dissertation, Loughborough University, 1994.

[13] D. R. Morgan, "Analysis and Realization of an Exponentially-Decaying Impulse Response Model for Frequency-Selective Fading Channels," *IEEE Signal Process. Lett.*, vol. 15, pp. 441–444, May. 2008.

[14] B. Zheng, C. You, and R. Zhang, "Fast Channel Estimation for IRS-Assisted OFDM," *IEEE Wireless Commun. Lett.*, vol. 10, no. 3, pp. 580–584, Mar. 2021.

[15] H. Li, R. Liu, M. Liy, Q. Liu, and X. Li, "IRS-enhanced wideband MU-MISO-OFDM communication systems," in *Proc. 2020 IEEE Wireless Commun. and Networking Conf. (WCNC'20)*, May. 2020, pp. 1–6.